Research Article | Vol. 29, No. 21 / 11 Oct 2021 / Optics Express 33456
Optics EXPRESS

Broadband thin-film and metamaterial absorbers using refractory vanadium nitride and their thermal stability

Wenhao Wang,[1,8] Hanbin Wang,[2,3,8] Peng Yu,[4,9] Kai Sun,[5] Xin Tong,[1] Feng Lin,[1] Cuo Wu,[1] Yimin You,[1] Wuze Xie,[2,3] Yunpeng Li,[2,3] Chenzhi Yuan,[1] Alexander O. Govorov,[6] Otto L. Muskens,[5] Hongxing Xu,[7] Song Sun,[2,3,10] and Zhiming Wang[1,11]

[1]*Institute of Fundamental and Frontier Sciences, University of Electronic Science and Technology of China, Chengdu 610054, China*
[2]*Microsystem and Terahertz Research Center, China Academy of Engineering Physics, Chengdu 610200, China*
[3]*Institute of Electronic Engineering, China Academy of Engineering Physics, Mianyang 621999, China*
[4]*College of Optoelectronic Technology, Chengdu University of Information Technology, Chengdu 610225, China*
[5]*Physics and Astronomy, Faculty of Engineering and Physical Sciences, University of Southampton, Southampton SO17 1BJ, UK*
[6]*Department of Physics and Astronomy, Ohio University, Athens, Ohio 45701, USA*
[7]*School of Physics and Technology, Center for Nanoscience and Nanotechnology, and Key Laboratory of Artificial Micro and Nanostructures of Ministry of Education, Wuhan University, Wuhan 430072, China*
[8]*These authors contributed equally to this work*
[9]*ypeng@cuit.edu.cn*
[10]*sunsong_mtrc@caep.cn*
[11]*zhmwang@uestc.edu.cn*

Abstract: Strong absorption of the full spectrum of sunlight at high temperatures is desired for photothermal devices and thermophotovoltaics. Here, we experimentally demonstrate a thin-film broadband absorber consisting of a vanadium nitride (VN) film and a SiO_2 anti-reflective layer. Owing to the intrinsic high loss of VN, the fabricated absorber exhibits high absorption over 90% in the wide range of 400-1360 nm. To further enhance the near-infrared absorption, we also propose a metamaterial absorber by depositing patterned VN square patches on the thin-film absorber. An average absorption of 90.4% over the range of 400-2500 nm is achieved due to the excitation of broad electric dipole resonance. Both thin-film and metamaterial absorbers are demonstrated to possess excellent incident angle tolerances (up to 60°) and superior thermal stability at 800 °C. The proposed refractory VN absorbers may be potentially used for solar energy harvesting, thermal emission, and photodetection.

1. Introduction

Solar energy could be harvested by a photovoltaic (PV) approach where the incident light directly excites electron-hole pairs in a semiconductor and generates electric current under external bias, or by a solar-thermal approach where sunlight is absorbed and converted to heat to drive related applications [1,2]. Broadband solar absorbers are critical for both strategies to maximize their energy utilization. Driven by surface plasmon excitations, noble metals are usually utilized to enhance light absorption [3–5]. However, the resonant nature of plasmon excitation limits the absorption bandwidth and requires complex multi-resonance antenna designs. Diverse structural configurations have been developed to achieve broadband absorption, including multi-stacked

#439546 https://doi.org/10.1364/OE.439546
Journal © 2021 Received 3 Aug 2021; revised 17 Sep 2021; accepted 22 Sep 2021; published 29 Sep 2021

Optics EXPRESS

planar absorber, metamaterial absorber (MMA), thin-film nanoparticles and nanocomposites absorber [6–16].

Solar thermal technologies, such as thermoelectric generators, thermophotovoltaics (TPV), thermal desalination, and thermionics, usually operate at high temperatures over 1000 °C [1,7,17–19]. For example, a solar TPV (STPV) system, in which sunlight is absorbed to heat the emitter, followed by the radiation of thermal photons towards the PV cell, generally works at the temperature of at least 800 °C [19,20]. Therefore, the ideal solar absorbers should not only be able to capture the full spectrum of sunlight but also have excellent thermal stability. Noble plasmonic metals possess relatively low melting points (1063 °C for bulk Au and 961 °C for Ag [21]), which decrease further when they are nanostructured [22]. Therefore, they can hardly meet the latter criteria. Recently, refractory materials have drawn much attention due to their high melting points (> 2000 °C) [21]. In [9], Li *et al.* demonstrated a broadband MMA using refractory titanium nitride (TiN). Due to the excellent thermal stability of TiN, an average absorption of 95% is preserved in the range of 400-800 nm even when the structure was annealed at 800 °C. Refractory tungsten (W) was also investigated to achieve strong absorption over 90% from 200 to 900 nm by forming periodic W cylinders [23]. However, the absorption bandwidths of these works are limited. It is still challenging to develop an absorber that can capture the full spectrum of sunlight while having excellent thermal stability. A few works have shown broader absorption bandwidth through a stacked SiC-W multilayer structure (absorption > 90% from 250 to 1650 nm) [7], or a SiO_2/TiN/SiO_2/Ti/SiO_2/Au configuration (absorption > 90% from 516 nm to 2696 nm) [13]. Nevertheless, these structures are very complicated and usually accompanied by demanding fabrications, hindering the practical applications of refractory broadband solar absorbers.

Refractory vanadium nitride (VN), as a member of transition-metal nitrides, shares similar properties with TiN, including a high melting point, good chemical stability, and intrinsic high optical loss [24]. It has been theoretically studied to show the potential for broadband absorption [25]. Here, we first experimentally demonstrate a refractory broadband thin-film absorber (TFA) composed of a VN film and a SiO_2 anti-reflective layer. Unlike TiN, which only behaves as a lossy dielectric in short wavelengths [9], VN presents lossy dielectric features in a much wider range of 400-2500 nm. Due to the high lossy properties of VN, the fabricated TFA exhibits high absorption over 90% in the wide range of 400-1360 nm. The thin-film solution involves no lithography and patterning fabrication processes and is therefore advantageous for an affordable and large-scale fabrication. To further enhance the absorption in the near-infrared (NIR) region, we also proposed an MMA by depositing a periodic array of VN square patches on the TFA. The absorption bandwidth of the MMA is improved by 18% (400-1530 nm) and 45% (400-2460 nm) for absorptions above 90% and 80%, respectively, compared to the TFA. In addition, the absorption performance of TFA and MMA show great robustness against large incident angles up to 60° and high operating temperatures up to 800 °C.

2. Experimental section

2.1. Fabrication

The thin-film VN absorber was fabricated by a three-step deposition process: a 5 nm thick Ti adhesive layer was firstly deposited on the Si substrate by electron beam evaporation (HHV TF600); then a 300 nm thick VN film was deposited with RF Magnetron Sputtering (Alliance concept AC450); finally, a 100 nm thick SiO_2 layer was deposited by plasma-enhanced chemical vapor deposition (Oxford Plasmalab System100 PECVD). The MMA was patterned by electron beam lithography (Vistec EBPG-5200+) with E-beam resist PMMA. After sputtering a 100 nm VN film, the VN patterns were formed using lift-off in acetone for 8 hours, followed by a 5-min-megasonic cleaning. A schematic diagram of the fabrication process of TFA and MMA is

Optics EXPRESS

provided in Supplement 1, Fig. S1. The thermal stability investigation was carried by annealing the samples in a vacuum chamber (OTF-1500X-80) for 24 hours at 800 °C and 1000 °C.

2.2. Measurements

The morphology of the VN film was investigated using atomic force microscopy (AFM) operating in contact mode (MFP-3D Infinite AFM). The scanning electron microscopy (SEM) images were taken by a GeminiSEM 300 from Carl Zeiss Microscopy GmbH. The permittivity of VN was retrieved from a thin film sample via a spectroscopic ellipsometer (Sentech SE850). The reflection of all the fabricated absorbers was measured using two different setups in separate ranges, 400-1400 nm, and 1400-2500 nm. Fourier transform infrared microscopy (FTIR, Thermo-Nicolet Nexus 670, Continuum microscope) was used for the 1400-2500 nm spectral range, using a ×15 optical objective with a numerical aperture of 0.58 and an MCT detector. The CaF_2 beamsplitter and IR source were used and the reflectance was normalized with an aluminum mirror. The investigated spot size on the sample was around 100×100 μm^2 for each measurement. For the visible and near-infrared spectral range, a total reflectance setup was used using a $BaSO_4$-coated integrating sphere with standard 8° reflectance port arrangement (Bentham) to capture both the specular and diffuse reflectance components. Light from the integrating sphere output was detected using a pair of Si and InGaAs spectrometers equipped with thermoelectrically cooled CCD arrays (Andor Shamrock & iDus). Light from a supercontinuum light source (Fianium SC400-1) covering the spectral range from 400-2300 nm was reduced in power to around 10 mW and was focused to a 30 μm diameter illumination spot onto the sample using a 20 cm focusing lens. Two-dimensional scans of the surface were performed using motorized stages (Thorlabs) to obtain spectra for the individual arrays. Reflectivity was obtained by normalizing to the spectrum of a $BaSO_4$ reference. A small difference of a few percent in absorption between the two setups is attributed to the different illumination geometries with the FTIR microscope offering a higher range of oblique angles than the 8° total reflectance setup.

2.3. Simulation

The full-field electromagnetic simulations were performed using commercial software FDTD Solutions. Periodic boundary conditions were employed along the x and y directions. Perfectly matched layers were applied along the z direction. A plane wave was incident from the top of the absorber and propagated along the z direction. The mesh size was 1 nm^3, and the mesh accuracy was 3 to ensure the accuracy of the results. The reflection (R) was obtained by a 2D frequency-domain power monitor placed above the incident source. The thickness of VN film is set as 300 nm to prevent the transmission of the device and thus enabling VN film as a mirror (detailed information about the effect of VN film's thickness on the absorption and transmission spectra of TFA and MMA is provided in Supplement 1, Fig. S2). The absorption was obtained by $A = 1 - R$. The permittivity of VN used in the simulation was from the measured results (Supplement 1, Fig. S3). The permittivities of TiN and Si were extracted from Pflüger [24] and Palik [26]. The permittivities of air and SiO_2 were set as 1 and 2.1, respectively. Since all the materials studied here are not magnetic, their permeabilities were set as 1.

3. Results and discussion

3.1. Thin-film VN absorber

Figure 1(a) shows the thin-film VN absorber (4.5 cm wide × 4 cm height), fabricated by a three-step deposition process (see Experimental section). The surface of the absorber looks very dark since most of the incident light is absorbed and the reflection is very low in the visible (Vis) range. The absorber comprises a VN film and a SiO_2 layer, deposited on Si substrate (inset of Fig. 1(b)). The measured spectrum shows that over 90% (80%) incident light is absorbed in the

Optics EXPRESS

wide range of 400-1360 (400-1820) nm (Fig. 1(b)). The sudden small drop in the absorption of around 0.031 at 1400 nm is originated from the difference between two measuring systems—the measured results consist of two spectra from 400 to 1400 nm and from 1400 to 2500 nm (see Experimental section). The excellent absorption performance of thin-film VN absorber is comparable with those of reported refractory broadband absorbers with metasurface structures [9,23]. Nevertheless, the lithography-free fabrication process enables the thin-film VN absorber in large-scale devices and practical applications.

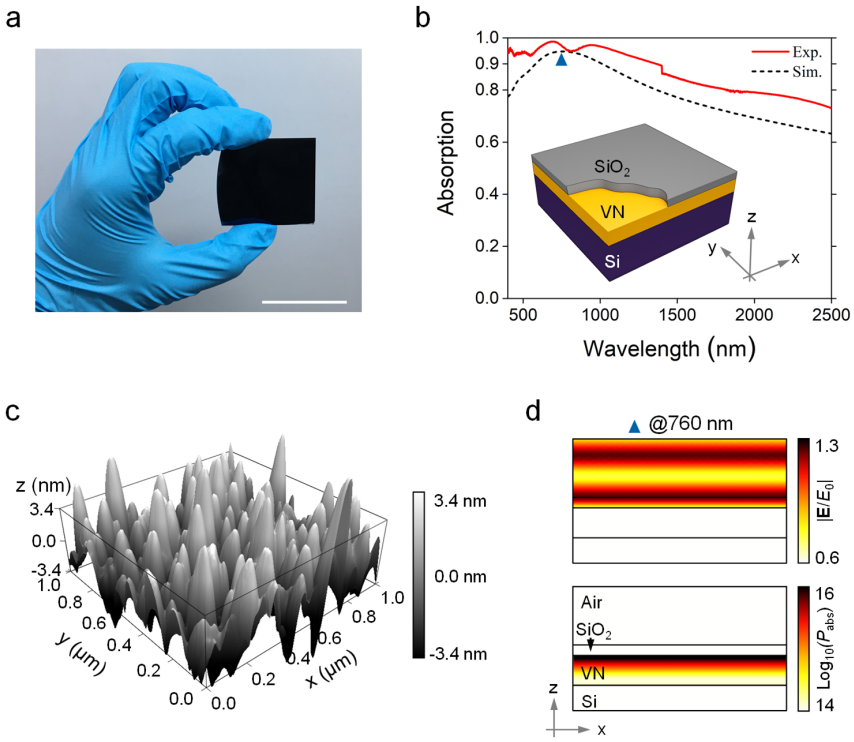

Fig. 1. Thin-film VN absorber. a, Camera image of large-scale TFA deposited on Si substrate. Scale bar: 4 cm. b, Simulated and measured absorption spectra of TFA. The inset shows the schematic of TFA. The thickness of the VN and SiO_2 layer are 300 and 100 nm, respectively. c, 3D atomic force microscopy image of 300 nm thick VN film. The root mean square roughness of the film is 2.447 nm. d, Simulated electric field and absorbed incident power distributions of TFA at 760 nm, marked as a blue triangle in b.

Electromagnetic simulations were performed to investigate the mechanism of the absorption performance of TFA, using commercial software FDTD Solutions (see Experimental section for more details). The local absorbed-power density of a non-magnetic material can be obtained by the formula:

$$P_{\text{abs}} = \frac{1}{2}\omega\varepsilon''|\mathbf{E}|^2, \tag{1}$$

where ω is the angular frequency, ε'' is the imaginary part of material's permittivity, and $\mathbf{E}$ is the electric field inside the material. The simulated absorption spectrum agrees well with the measured result (Fig. 1(b)). The relatively stronger absorption in experiments is attributed to the enhanced light-absorber interaction induced by the rough surface of the fabricated device [27]. As shown in Fig. 1(c), the VN film is composed of VN grains with a diameter of 30~80 nm and the root mean square (RMS) roughness of the film is 2.447 nm. An atomic force microscopy image

Optics EXPRESS

of the VN film with a larger area is shown in Supplement 1, Fig. S4. When the sunlight incident from the top surface of the TFA, it is multi-scattered by the VN particles, leading to enhanced absorption. Figure 1(d) shows the electric field and absorbed incident power distributions at 760 nm. Most of the incident power dissipated at the top surface of VN. The high absorption of the device is mainly originated from the intrinsic high loss of VN. Interestingly, unlike TiN, which only behaves as a lossy dielectric in short wavelengths [9], VN presents high lossy dielectric features in a much wider range of 400-2500 nm (see the permittivity of VN in Supplement 1, Fig. S3). Therefore, with the same structure configuration, the VN absorber shows strong absorption in the full solar spectrum, while the TiN absorber only exhibits high absorption in the wavelength below 500 nm (Supplement 1, Fig. S5). Also, the SiO_2 layer functioning as a typical anti-reflective layer lowers the refractive index contrast between the absorber and air, and dramatically increases the device's absorption by 11.6% (from 67.2% to 78.8%) over the whole solar spectrum (Supplement 1, Fig. S5).

3.2. Metamaterial VN absorber

Although the TFA works as a near-black absorber below 1400 nm, its absorption drops to 79.2% at 2000nm. To further enhance the absorption in the NIR region, we proposed to use an MMA solution. As shown in Figs. 2(a) and 2(b), the metamaterial VN absorber consists of a back VN film, a SiO_2 middle layer, and a periodic array of VN patches with square lattice. The key geometrical parameters are $P = 1050$ nm, $w = 575$ nm, $t_1 = 300$ nm and $t_2 = t_3 = 100$ nm. The measured absorption and SEM image of the fabricated sample are depicted in Fig. 2(c). Over 90% (80%) of the incident electromagnetic wave is absorbed in the range of 400-1530 nm (400-2460 nm), which agrees well with the simulated result. Compared with the TFA, the absorption bandwidth of MMA is improved by 18% and 45% for absorptions above 90% and 80%, respectively. The electric field distributions are calculated at 1210 nm (Fig. 2(d)), at which the calculated absorption reaches a maximum of 98.2%. The electric field shows enhancement at the two sides of the top VN patch, presenting an electric dipole feature. The incident power is strongly absorbed by the top patches and the back VN film under the gap between the VN patches.

Figure 3(a) shows the measured absorption spectra of MMA with different side lengths w of the top VN patches. With the increase of w, the absorption below 900 nm slightly decreases, while it shows enhancement in the range of 1400-2500 nm. The difference between the two separately measured spectra (in the red and blue side of 1400 nm) shows a maximum of 3.4% at $w = 500$ nm, which is very small and thus negligible compared with the total absorption. The evolution of the simulated absorption spectra with the increase of w (Fig. 3(b)) is consistent with the experimental results. The remarkable enhancement in the long wavelengths is attributed to the excitation of broad electric dipole resonance, which can even be found at 2000nm (Supplement 1, Fig. S6). The sudden increase near 1050 nm is due to the coupling of the absorber with the lattice mode, which is originated from the diffraction of scattered light in the ordered VN patch array. The wavelength for the lattice mode of a metastructure with a periodic square lattice under normal incidence can be obtained by [28,29]

$$\lambda_{(i,j)} = \frac{nP}{\sqrt{i^2 + j^2}}, \tag{2}$$

where i and j are integers related to the orders of the lattice modes in the x and y directions, respectively. n is the refractive index of the medium of propagation (here the absorption is obtained from the reflection, and thus n is the refractive index of air), and P is the period of the array. Therefore, the first order of the lattice mode (1,0) gives rise to absorption enhancement at 1050 nm. The kinks near 740 and 470 nm are induced by the lattice modes (1,1) and (2,1), respectively. It also can be concluded from the electric field patterns (Supplement 1, Fig. S6).

Optics EXPRESS

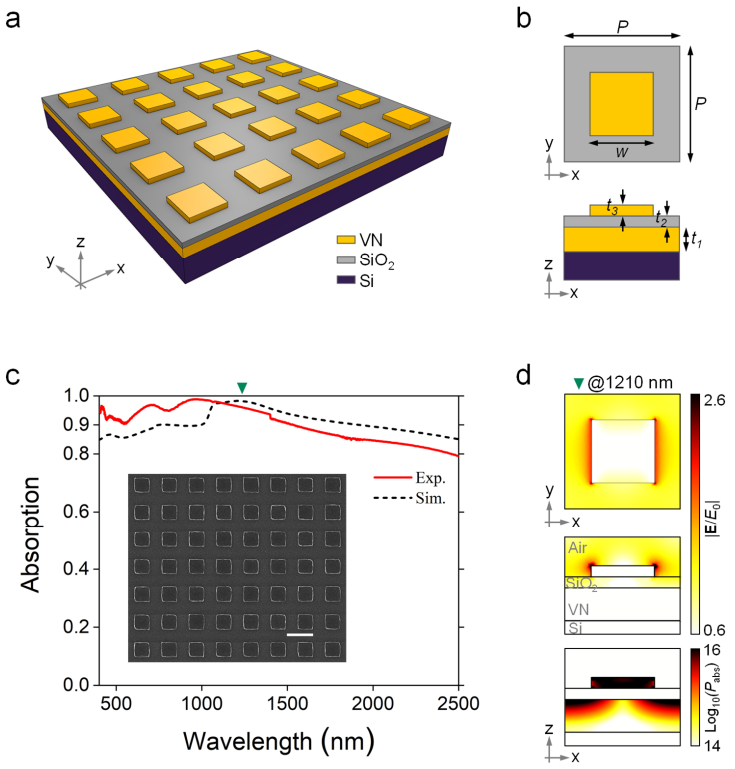

Fig. 2. Metamaterial VN absorber. a, The schematic of MMA composed of the top periodic VN square patches, SiO_2 film and VN film, deposited on Si substrate. b, Top and side view of the unit cell of MMA. The key geometrical parameters are $P = 1050$ nm, $w = 575$ nm, $t_1 = 300$ nm, $t_2 = 100$ nm and $t_3 = 100$ nm. c, Simulated and measured absorption spectra of MMA. The inset shows the SEM image of the fabricated MMA. Scale bar: 1 μm. d. Electric field and absorbed incident power distributions at 1210 nm, marked as a green inverted triangle in c.

When w is increased to 800 nm or even larger, the top VN layer can be viewed as a mirror, increasing the reflection and decreasing the absorption (Supplement 1, Fig. S7).

3.3. *High thermal stability of the VN absorber*

To investigate the thermal stability of the VN absorber, TFA and MMA were annealed in a vacuum chamber at 800 °C and 1000 °C for 24 hours. Figures 4(a) and 4(b) show that the MMA sample retains its shape when annealed at 800 °C, while the top VN patches heated at 1000 °C are melted into nanoparticles. Although the melting point of bulk VN (2077 °C) [30] is much higher than 1000 °C, it drops dramatically at the nanoscale dimension [22]. The absorption of TFA and MMA are nearly unchanged when annealed at 800 °C. The litter improvement of the absorption of TFA and MMA in the short wavelength and near 1500 nm is due to the small change of the optical properties of VN film that occurred at high temperatures. Similar properties have also been found in other refractory material-based absorbers [31,32]. As the annealing temperature increases to 1000 °C, the melted VN particles cause the diminishment of dipole resonance in the long wavelengths and lead to the resemblance of the absorption of MMA and TFA. The decrease of the absorption of TFA in the long wavelengths, dropping from 79.2% to 68.4% at 2000nm,

Optics EXPRESS

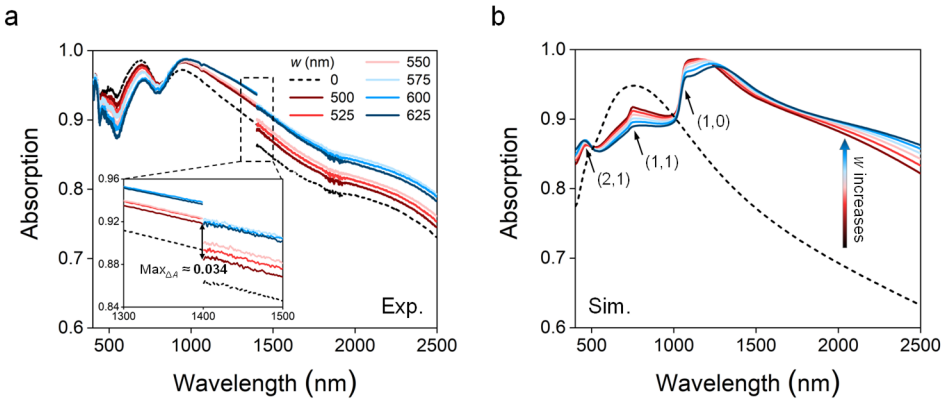

Fig. 3. Influence of the side length of the top VN patches on the absorption performance of MMA. a, Measured and b, simulated absorption spectra of MMA with different w. The measured absorption spectrum consists of two spectra from 400 to 1400 nm and 1400 to 2500 nm and shows a small discontinuity at 1400 nm. The inset shows the zoomed-in spectra near 1400 nm, and the maximum difference between the spectra below and above 1400 nm is 3.4% when $w = 500$ nm.

might be due to the diffusion and deformation of VN under the SiO_2 layer and the change of SiO_2's refractive index at high temperatures [33].

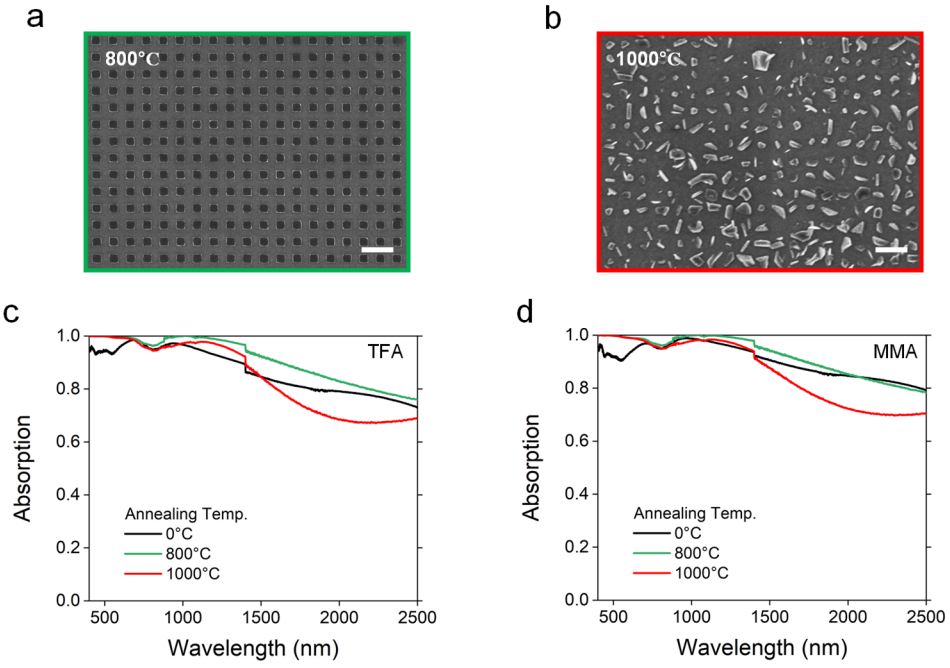

Fig. 4. Thermal stability of TFA and MMA. SEM images of MMA after annealing at a, 800 °C and b, 1000 °C for 24 hours. Scale bars: 1 μm. Measured absorption spectra of c, TFA and d, MMA ($w = 575$ nm) after annealing at different temperatures.

Optics EXPRESS

3.4. *Polarization and incident angle-insensitive absorption performance of the VN absorber*

For an ideal solar absorber, polarization and incident angle-independent absorption is desired. Due to the 90° rotational symmetry around the z axis (C_4), the proposed MMA shows polarization-independent absorption at normal incidence, like the TFA (Supplement 1, Fig. S8 and Fig. S9). Figure 5 plots the simulated absorption spectra of TFA and MMA for transverse electric (TE) and transverse magnetic (TM) polarizations. It can be seen that TFA maintains broadband high absorption for an oblique angle up to 60° for TE polarization. For TM polarization, strong absorption over 80% in the whole solar spectrum can be obtained even at an oblique angle up to 70°. The incident angle-insensitive absorption of TFA is attributed to the intrinsic lossy dielectric properties of VN, which can be concluded from the large imaginary part of VN's permittivity (Supplement 1, Fig. S3). It does not require specific excitation conditions and thus leads to high absorption even at large incident angles. The incident angle-insensitive absorption has also been demonstrated in lossy TiN-based absorber [9]. The MMA shows an enhanced absorption and improved robustness against incident angles over TFA in the long wavelengths due to the excited broad electric dipole resonances for both TE and TM polarizations. The first order of lattice mode is observed in the absorption spectrum of MMA, and its wavelength shows incident angle-dependent feature. Compared with broadband plasmonic absorbers, whose absorption is induced by surface plasmon and it is usually sensitive to the polarization and incident angle due to the resonant nature of surface plasmon [34], broadband VN absorber is promising in the applications where solar absorption is required to be robust against polarization and incident angles (such as STPV).

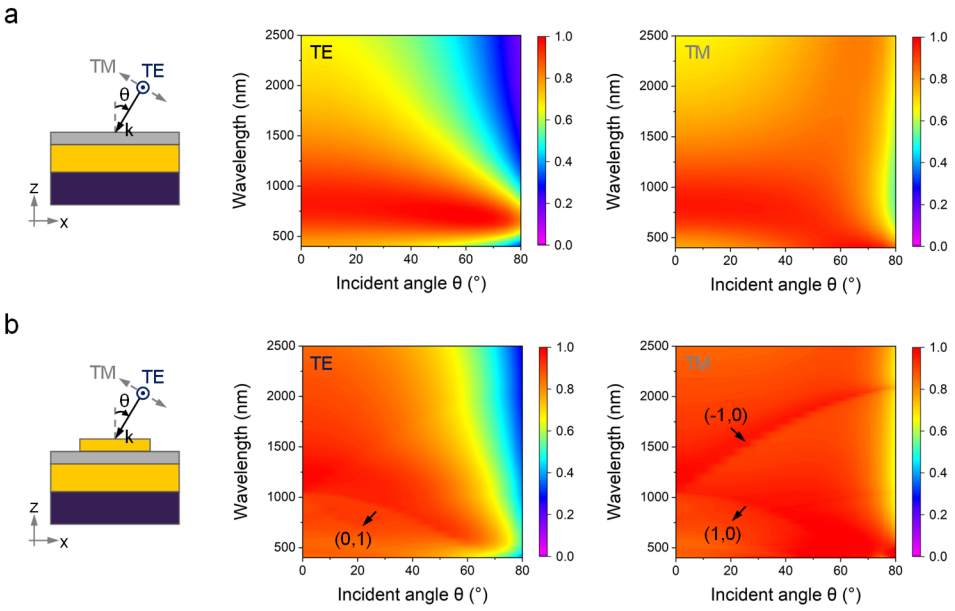

Fig. 5. Influence of the incident angle on the absorption performance of TFA and MMA. Simulated absorption spectra of a, TFA and b, MMA for various oblique incident angles, θ, for TE- and TM-polarized electromagnetic waves.

Optics EXPRESS

3.5. Comparison with selected experimental works of the broadband absorber

Finally, we compare the absorption performance of TFA and MMA with those of other prominent experimental works. As shown in Table 1, the absorption bandwidths in our work, including TFA and MMA, are comparable with that of the other broadest absorbers. Although the bandwidth of absorption > 90% is larger than 3 μm in [14] and [3], they mainly target the applications in near- and mid-infrared wavelength, and the visible range is not covered. In [13], it shows near 100% absorption in a broad range in the solar spectrum. However, the complicated structure and followed demanding fabrications hinder it in practical applications. Our proposed TFA is lithography-free and only needs a three-step deposition process, enabling large-scale functional devices. Also, the TFA and MMA show excellent thermal stability in high temperatures, comparable with that of refractory TiN- and W-based absorbers [7,9,23].

Table 1. Selected experimental works of Vis-NIR broadband absorbers

Ref.	Operating Wavelength (μm)	Bandwidth (μm)		Lithography-free	Material configuration	Working temperature (°C)
		A > 80%	A > 90%			
TFA	0.4 ~ 2.5	1.42	0.96	Yes	VN + SiO_2	800
MMA		2.06	1.13	No		
[11]	0.4 ~ 0.75	> 0.35	0.35	Yes	Au + SiO_2	-
[9]	0.4 ~ 0.8	> 0.4	~ 0.35	No	TiN + SiO_2	800
[23]	0.2 ~ 0.9	> 0.7	0.7	No	SiC + W + SiO_2	600
[12]	0.9 ~ 2.1	~ 1.1	0.925	No	Ti + Au + SiO_2	-
[35]	0.4 ~ 2.1	~ 1.4	~ 1.2	No	Mxene + Au + Al_2O_3	-
[7]	0.25 ~ 2.5	~ 1.65	~ 1.4	Yes	SiC + W + SiO_2	777
[13]	0.3 ~ 3	~ 2.5	2.18	No	TiN + Ti + Au + SiO_2	-
[3]	1.5 ~ 5	~ 3.5	3.04	No	Pd + Polyimide	-
[14]	1 ~ 5	3.8	3.2	No	Cr + SiO_2	-

4. Conclusion

In summary, we demonstrated a TFA and an MMA using refractory VN. Owing to the high lossy properties of VN and anti-reflection of the SiO_2 layer, the TFA exhibits high absorption over 90% in the range of 400-1360 nm. The lithography-free fabrication process makes the TFA promising in large-scale devices. The MMA was demonstrated by patterning VN square patches onto the TFA. Due to the excitation of broad electric dipole resonance in long wavelengths, the absorption bandwidth is improved by 18% and 45% for absorptions over 90% and 80%, respectively. The absorption performance of TFA and MMA are insensitive to polarization angles at normal incidence and are robust to large incident angles (up to 60° for TE and 70° for TM polarization). Besides, the TFA and MMA have excellent thermal stability and almost unchanged absorption performance at an annealing temperature of 800 °C. The broadband refractory VN absorber reported here can be potentially used in thermophotovoltaics and other solar thermal applications.

Funding. National Key Research and Development Program of China (2019YFB2203400, 2019YFE0121600); China Postdoctoral Science Foundation (2019M663467); Sichuan Province Science and Technology Support Program (2020YJ0041, 2021YFH0054); National Natural Science Foundation of China (62005037, 62005256); Foundation of CAEP Ultra-precision Machining Technology Key Laboratory (ZM18008); CAEP Innovation and Development Grant (CX20200011).

Acknowledgments. H. B. W and S. S. acknowledge assistance from Li Liu and Su Yan in device fabrication and Dechao Meng in AFM measurements.

Optics EXPRESS

Disclosures. The authors declare no conflicts of interest.

Data availability. The datasets generated and analyzed during the current study are available from the authors upon reasonable request.

Supplemental document. See Supplement 1 for supporting content.

References

1. M. Thirugnanasambandam, S. Iniyan, and R. Goic, "A review of solar thermal technologies," Renewable Sustainable Energy Rev. **14**, 312–322 (2010).
2. N. Kannan and D. Vakeesan, "Solar energy for future world: - A review," Renewable Sustainable Energy Rev. **62**, 1092–1105 (2016).
3. J. A. Bossard, L. Lin, S. Yun, L. Liu, D. H. Werner, and T. S. Mayer, "Near-Ideal Optical Metamaterial Absorbers with Super-Octave Bandwidth," ACS Nano **8**, 1517–1524 (2014).
4. K. Aydin, V. E. Ferry, R. M. Briggs, and H. A. Atwater, "Broadband polarization-independent resonant light absorption using ultrathin plasmonic super absorbers," Nat. Commun. **2**, 517 (2011).
5. B. Wang, P. Yu, W. Wang, X. Zhang, H.-C. Kuo, H. Xu, and Z. M. Wang, "High-Q Plasmonic Resonances: Fundamentals and Applications," Adv. Opt. Mater. **9**(7), 2001520 (2021).
6. C. M. Watts, X. Liu, and W. J. Padilla, "Metamaterial Electromagnetic Wave Absorbers," Adv. Mater. **24**, OP98–OP120 (2012).
7. A. Raza, A. S. Alketbi, R. Devarapalli, H. Li, and T. Zhang, "Refractory Ultrathin Nanocomposite Solar Absorber with Superior Spectral Selectivity and Thermal Stability," Adv. Opt. Mater. **8**, 2000679 (2020).
8. P. Yu, L. V. Besteiro, Y. Huang, J. Wu, L. Fu, H. H. Tan, C. Jagadish, G. P. Wiederrecht, A. O. Govorov, and Z. Wang, "Broadband Metamaterial Absorbers," Adv. Opt. Mater. **7**, 1800995 (2019).
9. W. Li, U. Guler, N. Kinsey, G. V. Naik, A. Boltasseva, J. Guan, V. M. Shalaev, and A. V. Kildishev, "Refractory Plasmonics with Titanium Nitride: Broadband Metamaterial Absorber," Adv. Mater. **26**, 7959–7965 (2014).
10. J. Zou, P. Yu, W. Wang, X. Tong, L. Chang, C. Wu, W. Du, H. Ji, Y. Huang, X. Niu, A. O. Govorov, J. Wu, and Z. Wang, "Broadband mid-infrared perfect absorber using fractal Gosper curve," J. Phys. D: Appl. Phys. **53**, 105106 (2019).
11. M. K. Hedayati, M. Javaherirahim, B. Mozooni, R. Abdelaziz, A. Tavassolizadeh, V. S. K. Chakravadhanula, V. Zaporojtchenko, T. Strunkus, F. Faupel, and M. Elbahri, "Design of a Perfect Black Absorber at Visible Frequencies Using Plasmonic Metamaterials," Adv. Mater. **23**, 5410–5414 (2011).
12. F. Ding, J. Dai, Y. Chen, J. Zhu, Y. Jin, and S. I. Bozhevolnyi, "Broadband near-infrared metamaterial absorbers utilizing highly lossy metals," Sci. Rep. **6**, 39445 (2016).
13. F. Qin, X. Chen, Z. Yi, W. Yao, H. Yang, Y. Tang, Y. Yi, H. Li, and Y. Yi, "Ultra-broadband and wide-angle perfect solar absorber based on TiN nanodisk and Ti thin film structure," Sol. Energy Mater. Sol. Cells **211**, 110535 (2020).
14. H. Deng, L. Stan, D. A. Czaplewski, J. Gao, and X. Yang, "Broadband infrared absorbers with stacked double chromium ring resonators," Opt. Express **25**, 28295–28304 (2017).
15. S. Guo, C. Hu, and H. Zhang, "Unidirectional ultrabroadband and wide-angle absorption in graphene-embedded photonic crystals with the cascading structure comprising the Octonacci sequence," J. Opt. Soc. Am. B **37**, 2678–2687 (2020).
16. Y. Ma, T. Zhang, M. Mao, D. Zhang, and H. Zhang, "Switchable multifunctional modulator realized by the stacked graphene-based hyperbolic metamaterial unit cells," Opt. Express **28**, 39890–39903 (2020).
17. W. Baoqing, W. Wenhao, A. Eric, Z. Xutao, Y. Peng, X. Hongxing, and W. Zhiming, "Broadband refractory plasmonic absorber without refractory metals for solar energy conversion," J. Phys. D: Appl. Phys. **54**(9), 094001 (2020).
18. J. W. Schwede, T. Sarmiento, V. K. Narasimhan, S. J. Rosenthal, D. C. Riley, F. Schmitt, I. Bargatin, K. Sahasrabuddhe, R. T. Howe, J. S. Harris, N. A. Melosh, and Z. X. Shen, "Photon-enhanced thermionic emission from heterostructures with low interface recombination," Nat. Commun. **4**, 1576 (2013).
19. A. Lenert, D. M. Bierman, Y. Nam, W. R. Chan, I. Celanović, M. Soljačić, and E. N. Wang, "A nanophotonic solar thermophotovoltaic device," Nat. Nanotechnol. **9**, 126–130 (2014).
20. P. Nagpal, S. E. Han, A. Stein, and D. J. Norris, "Efficient Low-Temperature Thermophotovoltaic Emitters from Metallic Photonic Crystals," Nano Lett. **8**, 3238–3243 (2008).
21. U. Guler, A. Boltasseva, and V. M. Shalaev, "Refractory Plasmonics," Science **344**, 263 (2014).
22. Z. Zhang, J. C. Li, and Q. Jiang, "Modelling for size-dependent and dimension-dependent melting of nanocrystals," J. Phys. D: Appl. Phys. **33**, 2653–2656 (2000).
23. Y. Huang, L. Liu, M. Pu, X. Li, X. Ma, and X. Luo, "A refractory metamaterial absorber for ultra-broadband, omnidirectional and polarization-independent absorption in the UV-NIR spectrum," Nanoscale **10**, 8298–8303 (2018).
24. J. Pflüger, J. Fink, W. Weber, K. P. Bohnen, and G. Crecelius, "Dielectric properties of TiCx, TiNx, VCx, and VNx from 1.5 to 40 eV determined by electron-energy-loss spectroscopy," Phys. Rev. B **30**, 1155–1163 (1984).
25. M. C. Soydan, A. Ghobadi, D. U. Yildirim, V. B. Erturk, and E. Ozbay, "All Ceramic-Based Metal-Free Ultra-broadband Perfect Absorber," Plasmonics **14**, 1801–1815 (2019).
26. E. D. Palik, *Handbook of optical constants of solids* (Academic press, 1998).

Optics EXPRESS

27. C.-C. Chen, S. H. Chang, L.-C. Chen, F.-S. Kao, H.-M. Cheng, S.-C. Yeh, C.-T. Chen, W.-T. Wu, Z.-L. Tseng, C. L. Chuang, and C.-G. Wu, "Improving the efficiency of inverted mixed-organic-cation perovskite absorber based photovoltaics by tailing the surface roughness of PEDOT: PSS thin film," Sol. Energy **134**, 445–451 (2016).
28. L. Rayleigh, "On the Dynamical Theory of Gratings," *Proceedings of the Royal Society of London. Series A, Containing Papers of a Mathematical and Physical Character* **79**, 399–416 (1907).
29. T. W. W. Maß and T. Taubner, "Incident Angle-Tuning of Infrared Antenna Array Resonances for Molecular Sensing," ACS Photonics **2**, 1498–1504 (2015).
30. A. B. Mei, O. Hellman, N. Wireklint, C. M. Schlepütz, D. G. Sangiovanni, B. Alling, A. Rockett, L. Hultman, I. Petrov, and J. E. Greene, "Dynamic and structural stability of cubic vanadium nitride," Phys. Rev. B **91**, 054101 (2015).
31. H. Wang, V. Prasad Sivan, A. Mitchell, G. Rosengarten, P. Phelan, and L. Wang, "Highly efficient selective metamaterial absorber for high-temperature solar thermal energy harvesting," Sol. Energy Mater. Sol. Cells **137**, 235–242 (2015).
32. S. Han, J.-H. Shin, P.-H. Jung, H. Lee, and B. J. Lee, "Broadband Solar Thermal Absorber Based on Optical Metamaterials for High-Temperature Applications," Adv. Opt. Mater. **4**, 1265–1273 (2016).
33. Y. Ji, Y. Jiang, H. Liu, L. Wang, D. Liu, C. Jiang, R. Fan, and D. Chen, "Effects of thermal treatment on infrared optical properties of SiO2 films on Si Substrates," Thin Solid Films **545**, 111–115 (2013).
34. T. Søndergaard, S. M. Novikov, T. Holmgaard, R. L. Eriksen, J. Beermann, Z. Han, K. Pedersen, and S. I. Bozhevolnyi, "Plasmonic black gold by adiabatic nanofocusing and absorption of light in ultra-sharp convex grooves," Nat. Commun. **3**, 969 (2012).
35. K. Chaudhuri, M. Alhabeb, Z. Wang, V. M. Shalaev, Y. Gogotsi, and A. Boltasseva, "Highly Broadband Absorber Using Plasmonic Titanium Carbide (MXene)," ACS Photonics **5**, 1115–1122 (2018).